



# Superior mechanical resistance in the exoskeleton of the coconut crab, *Birgus latro*



T. Inoue<sup>a,\*</sup>, T. Hara<sup>a</sup>, K. Nakazato<sup>a</sup>, S. Oka<sup>b</sup>

<sup>a</sup> National Institute for Materials Science, 1-2-1, Sengen, Tsukuba 305-0047, Japan

<sup>b</sup> Okinawa Churashima Foundation, 888 Ishikawa, Motobu, Okinawa 905-0206, Japan

## ARTICLE INFO

### Keywords:

Biomineralization  
Tissue structure  
Crustacean cuticle  
Nanoindentation  
Structure-property relations

## ABSTRACT

The hierarchical tissue structure that can balance the lightweight and strength of organisms gives hints on the development of biologically inspired materials. The exoskeleton of the coconut crab, *Birgus latro*, which is the largest terrestrial crustacean, was systematically analyzed using a materials science approach. The tissue structures, chemical compositions, and mechanical properties of the claw, walking legs, cephalothorax, and abdomen were compared. The local mechanical properties, hardness ( $H$ ) and stiffness ( $E$ ), were examined by nanoindentation testing. The stacking height,  $Sh$ , of the twisted plywood structure observed only in the exocuticle, the exoskeleton thickness, and the thickness and compositions at each layer differed significantly by body part. The exocuticle is strongly mineralized regardless of body parts. The claw and walking legs were thicker than the cephalothorax and abdomen, and their endocuticle was mineralized as compared to the endocuticle in the cephalothorax and abdomen. The  $H$  and  $Sh$  had a correlation in the exocuticle layer, and the  $H$  increased with decreasing the  $Sh$ . On the  $H$ – $E$  map for abrasion resistance of materials, the results showed that the exocuticle layer of the coconut crab was superior to that of other arthropods and all engineering polymers and competitive with the hardest metallic alloys.

## 1. Introduction

Almost all organisms in the phylum Arthropod are covered by an exoskeleton. The exoskeleton is hard and lightweight, helps protect itself from dryness and enemies, and plays an important role in environmental adaptation. In various fields such as biology, engineering, and medicine, biomineralized tissues are a valuable source of design concepts for man-made materials and form the most important library of information on the evolution of life [1].

The exoskeleton in the arthropods is structurally heterogeneous, and it has very complicated hierarchical tissue [2–4], as shown in Fig. S1 in the supplementary material. This information has been revealed through advanced analytical equipment and technology. Basically, the exoskeleton is composed of four layers: the epicuticle (wax layer of the outermost surface), the exocuticle, the endocuticle, and the membranous (adjacent to cells) layers. Among these layers, the exocuticle and endocuticle are very hard and mineralized, but the mechanical properties vary significantly depending on the organism and the body part [5–8]. Fabritius et al. [5] examined the relationships among structure, component, and hardness in the exocuticle and the endocuticle of the exoskeleton

forming the dorsal carapace of the edible crab *Cancer pagurus* and clarified the existence of the complex structural organization and local gradients in component/hardness. The claws and cephalothorax (carapaces) of the American lobster, *Homarus americanus*, and the brown crab, *Cancer pagurus*, were analyzed via thermogravimetry and X-ray powder diffraction [6], which showed that the claw was strongly mineralized and very hard as compared with the cephalothorax, and the exoskeleton of the lobster is less mineralized (and therefore lighter and less hard) than that of the crab. It was concluded that these differences are related to the mechanical requirements and biological escape behaviors of the animals. During evolution, all parts of the exoskeleton in crustaceans are optimized to fulfill different functions by adapting the chemical composition and tissue structure under ambient conditions. The claws and carapaces may have developed significantly in the body to protect themselves, but there are very few studies on their differences from other body parts (legs and abdomen). We succeeded in creating a three-dimensional visualization of the complex claw tissue of the coconut crab, *Birgus latro*, which has a pinching force of more than 90 times its body weight and showed the correlation between the microstructure, hardness, and composition of the claw [9]. If only the claws had been strongly mineralized in their

\* Corresponding author.

E-mail address: [INOUE.Tadanobu@nims.go.jp](mailto:INOUE.Tadanobu@nims.go.jp) (T. Inoue).

<https://doi.org/10.1016/j.mtbio.2021.100132>

Received 5 July 2021; Received in revised form 6 August 2021; Accepted 31 August 2021

Available online 8 September 2021

2590-0064/© 2021 The Author(s). Published by Elsevier Ltd. This is an open access article under the CC BY-NC-ND license (<http://creativecommons.org/licenses/by-nc-nd/4.0/>).

body over the course of the coconut crabs evolution, the mechanical properties, components, and tissues in other parts of the exoskeleton likely would be significantly different from those of the claws. Besides, coconut crabs are terrestrial crustaceans and are likely to have characteristics that are different from those of the exoskeletons of underwater crustaceans and other organisms.

In this paper, we focus on differences in the mechanical properties of the coconut crab exoskeleton: the claw, the first walking leg, the front cephalothorax, the rear cephalothorax, and the abdomen. The local hardness,  $H$ , and stiffness,  $E$ , were examined via a nanoindentation test. The variations of tissue structures and chemical compositions related to the  $H$  and the  $E$  are discussed. The results were plotted on an  $H$ – $E$  map with data for many engineering materials and other organisms.

## 2. Materials and methods

### 2.1. Specimen preparation

The coconut crab was obtained from a local market in Naha City, Okinawa Island, in southwestern Japan. The coconut crab shown in Fig. 1 is male, and the body weight ( $BW$ ) and the thoracic length ( $ThL$ ) were 1,070 g and 62 mm, respectively. This crab is estimated to be a 20–23 years old adult from  $ThL$  [10]. Adult coconut crabs of the Okinawan population molt only once per year, during the winter dry season [10]. The crab was obtained in the summer of July, past half a year since the last molting. After euthanasia by deep freezing, the crab was moved to our laboratory in Tsukuba; there it was thawed under running water, and then each part, the left claw (CL), the first walking leg (1WL), the front cephalothorax (FC), the rear cephalothorax (RC), and the abdomen (AM), of the body shown in Fig. 1 was cut with a saw to fit within the dimensions of mounting cup used in the embedding process. Embedding cups were filled with epoxy (Struers, EPOFIX resin), and the samples were left to cure at room temperature for approximately 12 h. The samples were placed under vacuum for 10 min immediately after the addition of epoxy to further ensure penetration of epoxy into specimen voids. Then they were ground with Grit320/600/800 grade SiC papers, subsequently polished with 9, 3, and 1  $\mu\text{m}$  diamond suspension, and finally polished with 0.05  $\mu\text{m}$  alumina suspension. In order to observe the microstructure of each part, all samples were polished and coated with about 2 nm of osmium. After they finished, the specimens were re-polished and subjected to nanoindentation tests. The test piece for observing the fracture surface was cut from each part with a saw, and then it was broken by hitting the back of a chisel with a hammer. The pieces were placed in the air for more than 48 h before SEM observation.

### 2.2. Microstructure observation

We applied osmium coating on the sample surface, which is a popular method to add electron conductivity on a non-conductive sample to

obtain a clear image by eliminating electron charge up. An osmium coater apparatus made by Meiwafoods Co., Ltd., Japan, that the principle of the coating was a plasma CVD was used. Since the thickness of the coated osmium amorphous film is very thin, several nm, the effect on the compositional analysis by EDS is negligible. The microstructure and chemical composition on the polished surfaces were characterized using an optical microscope (OM) and focused ion beam (FIB)–scanning electron microscope (SEM; Thermo Fisher Scientific Scios 2) with energy-dispersive X-ray spectroscopy (EDS) using a large silicon-drift detector (Oxford Instruments Ultim Max 170 EDS). Fig. 2 shows SEM cross-sectional images of each part, CL, 1WL, FC, RC, and AM. The EDS found calcium (Ca), magnesium (Mg), phosphorus (P), carbon (C), and oxygen (O) to be the main components, and aluminum (Al), sodium (Na), and chloride ( $\text{Cl}^-$ ) in minor amounts [9]. Al is residue from the alumina used in the polishing. The other components may be due to the residual NaCl in the soil near the coast. These minor components, sodium, chloride, and silicon, are found in the exoskeleton of the lobster and the edible crab [6]. Quantitative analyses of the main components were conducted in the three areas enclosed by red rectangles associated with each layer, as shown in Fig. 2. The areas in the exocuticle and endocuticle corresponded to mid-thickness in each layer, and the intermediate area was positioned closer to the endocuticle than to the boundary line, where the contrast changed significantly. The fracture surface was observed by SEM (JEOL JSM-7900F; accelerating voltage: 2 kV; detector: ET-SE) coating with about 2 nm of osmium. The thickness of each layer, exocuticle, intermediate, and endocuticle, was determined through the SEM images of the polishing surfaces.

### 2.3. Nanoindentation tests

The mechanical testing was performed via nanoindentation testing using ELIONIX, ENT-NEXUS. It was performed at ambient temperature after polishing. For each layer, the test was performed five times in three areas marked by red rectangles, as seen in Fig. 2, and an area close to the surface (distance from the surface,  $x \approx 20 \mu\text{m}$ ) of the exocuticle. The samples for the dehydrated condition were placed in the air for more than 48 h before indentation. The tests were conducted under the dry samples with a Berkovich-type diamond indenter with an angle of  $115^\circ$  at a maximum force of 5 mN. The load function consisted of a 5-s loading to 5 mN, followed by a 5-s hold at that force, and then a 5-s unloading. The hardness ( $H$ ) and reduced modulus ( $E_r$ ) were analyzed from the unloading curve using the Oliver-Pharr method. Here, as in pioneering studies [11–14] on biological research,  $E_r$  was employed as the stiffness.

### 2.4. Density measurement

The three samples for each body part were cut with a saw. The density of the samples was measured by using a pycnometer method at temperatures of  $23\text{--}26^\circ\text{C}$  (SHIMAZU, AUW220D) on the basis of JIS Z 8807.

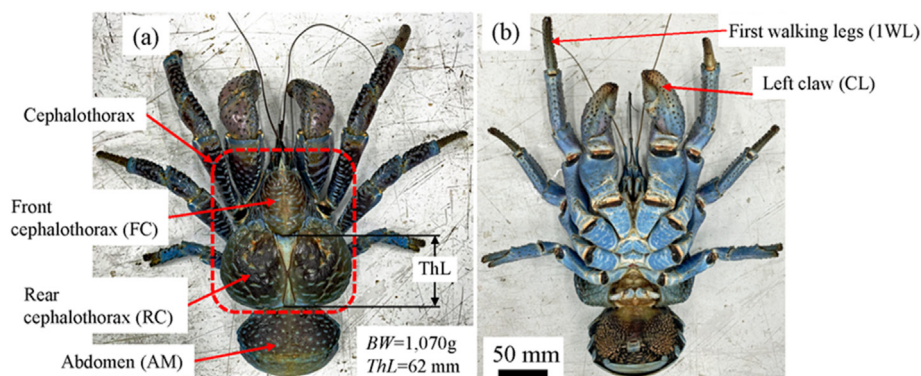


Fig. 1. Photographs of the (a) front and (b) back of the coconut crab, *Birgus latro*, used in the present study. Here,  $BW$  denotes body weight, and  $ThL$  denotes thoracic length.

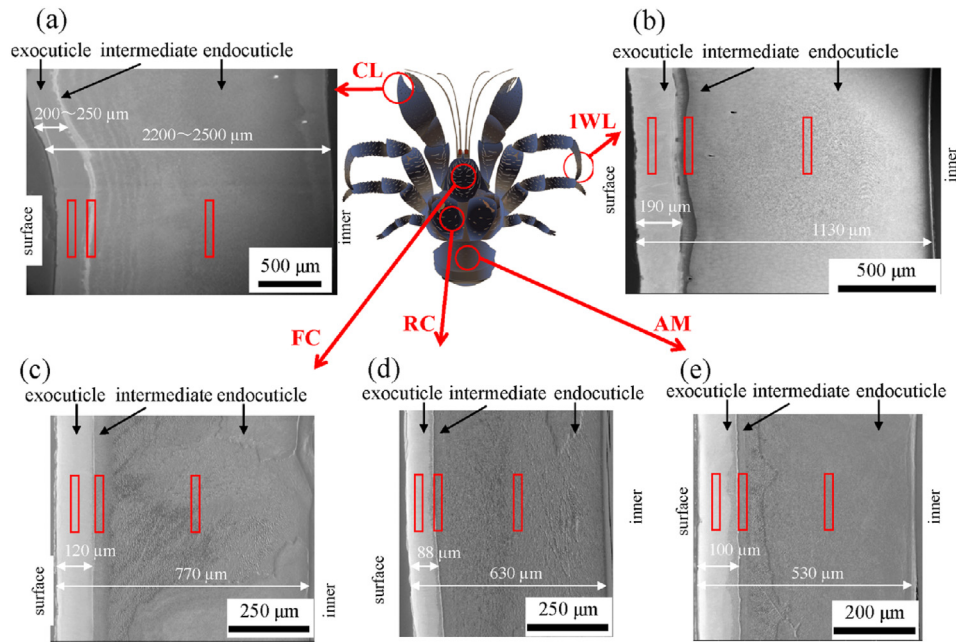


Fig. 2. Scanning electron microscope (SEM) cross-sectional images of the (a) claw, (b) first walking leg, (c) front cephalothorax, (d) rear cephalothorax, and (e) abdomen of the coconut crab used.

Since it was not possible to measure separately for each layer, the density of the exoskeleton of three samples for each body part is represented as average values.

### 3. Results

#### 3.1. Thickness and chemical composition of each layer

As shown in Fig. 2, the exocuticle layer and the endocuticle layer are clearly observed in all samples. Since it was difficult to perfectly judge the intermediate layer via only the SEM images shown in Fig. 2, its thickness was obtained via the high-magnification SEM images ( $\times 3,500$ ) shown in Fig. 3. The thickness and EDS results of each layer are summarized in Table 1.

The exoskeleton thickness depended on the measurement location. The maximum thickness of the CL was 2,600  $\mu\text{m}$ , of the 1WL was 1,400  $\mu\text{m}$  at WL, of the FC was 800  $\mu\text{m}$ , of the RC was 730  $\mu\text{m}$ , and of the AM was 610  $\mu\text{m}$ . In short, the claw is the thickest, and the abdomen is the thinnest. The claw and legs are thicker than the cephalothorax and the abdomen, and the AM is less than 1/4 as thick as the CL. The claw has the thickest exocuticle; its thickness accounted for 10% of the exoskeleton thickness [9]. Contrary to expectations, this rate is lower than the rate, 14~19%, of other parts. The exoskeleton of the coconut crab is much thicker than that of the blue crab, *Callinectes sapidus*, and the green crab *Carcinus aestuarii* [15]. For example, the exocuticle of the CL is more than four times thicker than that of the blue crab's red claw (25  $\mu\text{m}$ ) and the green crab's claw (47  $\mu\text{m}$ ), and the exoskeleton of the coconut crab is 10 times thicker than that of the green crab's claw (247  $\mu\text{m}$ ).

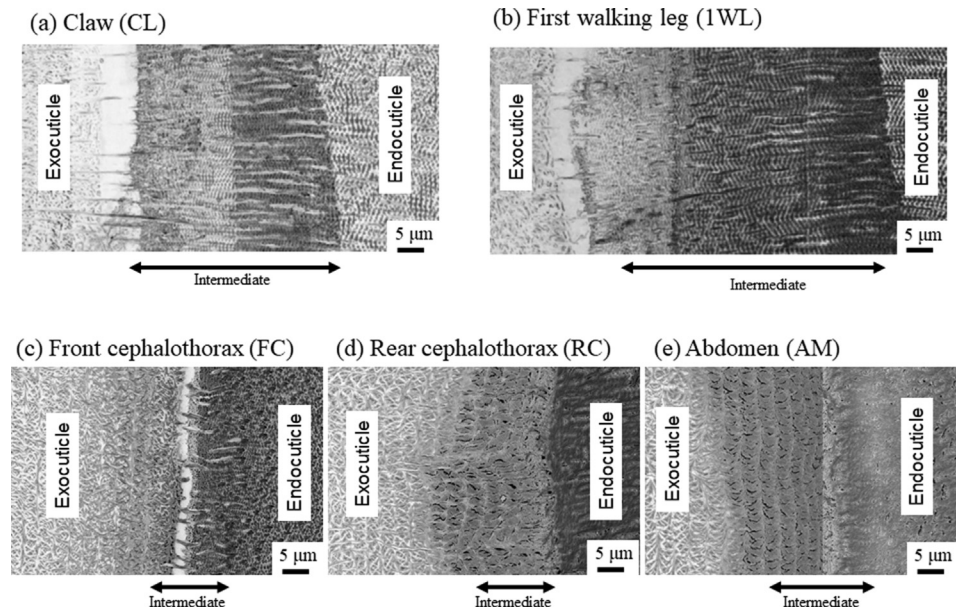


Fig. 3. SEM micrographs near the intermediate layer on (a) claw, (b) first walking leg, (c) front cephalothorax, (d) rear cephalothorax, and (e) abdomen of the coconut crab.

**Table 1**

Thickness and EDS results of three layers for all samples. Here, EDS results show weight % of calcium (Ca), magnesium (Mg), phosphorus (P), oxygen (O), and carbon (C). The compositions are the average values, including their standard deviation.

Sample	Layer	Thickness ( $\mu\text{m}$ )	Ca (wt%)	Mg (wt%)	P (wt%)	O (wt%)	C (wt%)
Claw (CL)	Exocuticle	200–250	$30.6 \pm 0.2$	$2.0 \pm 0.1$	$0.4 \pm 0.0$	$52.5 \pm 0.3$	$13.9 \pm 0.3$
	Intermediate	40	$22.4 \pm 0.2$	$1.5 \pm 0.1$	$2.1 \pm 0.1$	$51.1 \pm 0.3$	$21.3 \pm 0.3$
	Endocuticle	1900–2300	$23.8 \pm 0.2$	$1.6 \pm 0.1$	$0.5 \pm 0.0$	$49.5 \pm 0.3$	$23.3 \pm 0.3$
First walking leg (1WL)	Exocuticle	180–190	$31.0 \pm 0.1$	$1.8 \pm 0.0$	$0.4 \pm 0.0$	$51.4 \pm 0.1$	$14.7 \pm 0.1$
	Intermediate	50	$19.9 \pm 0.1$	$1.3 \pm 0.0$	$2.6 \pm 0.0$	$49.7 \pm 0.1$	$24.9 \pm 0.1$
	Endocuticle	1100–1150	$25.3 \pm 0.1$	$1.6 \pm 0.0$	$1.0 \pm 0.0$	$49.2 \pm 0.1$	$21.8 \pm 0.1$
Front cephalothorax (FC)	Exocuticle	115–125	$26.7 \pm 0.1$	$1.8 \pm 0.0$	$0.7 \pm 0.0$	$50.8 \pm 0.2$	$19.3 \pm 0.1$
	Intermediate	15	$20.5 \pm 0.1$	$1.2 \pm 0.0$	$2.6 \pm 0.0$	$49.2 \pm 0.2$	$24.7 \pm 0.2$
	Endocuticle	600–650	$12.6 \pm 0.1$	$0.6 \pm 0.0$	$0.8 \pm 0.0$	$46.9 \pm 0.2$	$34.8 \pm 0.2$
Rear cephalothorax (RC)	Exocuticle	75–90	$25 \pm 0.1$	$1.6 \pm 0.0$	$0.7 \pm 0.0$	$49.5 \pm 0.2$	$22.6 \pm 0.2$
	Intermediate	15	$15.7 \pm 0.1$	$1.0 \pm 0.0$	$2.2 \pm 0.0$	$48.8 \pm 0.2$	$29.8 \pm 0.2$
	Endocuticle	615	$9.1 \pm 0.1$	$0.4 \pm 0.0$	$0.4 \pm 0.0$	$46.7 \pm 0.2$	$38.1 \pm 0.2$
Abdomen (AM)	Exocuticle	95–105	$24.2 \pm 0.1$	$1.5 \pm 0.0$	$0.6 \pm 0.0$	$49.3 \pm 0.2$	$23.7 \pm 0.2$
	Intermediate	20	$15.9 \pm 0.1$	$0.9 \pm 0.0$	$3.1 \pm 0.0$	$45.8 \pm 0.2$	$31.4 \pm 0.3$
	Endocuticle	430–480	$14.8 \pm 0.1$	$0.6 \pm 0.0$	$0.5 \pm 0.0$	$46.7 \pm 0.2$	$33.6 \pm 0.2$

In all parts, the Ca concentrations and the Mg concentrations are highest at the exocuticle, while the C concentrations are lowest there. The Ca concentrations of the CL and 1WL are higher than those of other parts. Curiously, the P concentrations are highest at the intermediate layer. O concentrations are highest in the exocuticle, but there were no significant differences between layers and parts.

3.2. Fracture surface

Fig. 4 shows SEM micrographs of a fracture surface and a polished surface at two layers in the 1WL. Here, Fig. 4(b, e) shows enlarged micrographs at mid-thickness of the exocuticle layer. Two layers of exocuticle and endocuticle are clearly observed from the fracture surface (Fig. 4(a)). In the exocuticle (Fig. 4(b)), the twisted plywood pattern structure rotated 180° around an axis normal to the surface, which is characteristic of the cuticle of crustaceans [9,12]. It was formed by a certain stacking of the chitin–protein layers; its stacking height, *Sh*, was 1.6  $\mu\text{m}$ . This corresponds to the lamella thickness observed in Fig. 4(e). The fracture surface changes drastically in the intermediate (Fig. 4(c)). In the endocuticle (Fig. 4(d)), the pore canal tubules (pct) along deep

grooves parallel to the *x*-direction exist toward the surface from the inner layer, and relatively thin pct parallel to the *z*-directions from the regularly arranged pore canals (pc) at a spacing of 0.6  $\mu\text{m}$  are observed. In the polished surface at the same position (Fig. 4(f)), the inorganic layer covering the entire surface has a line parallel to the *y*-direction, and the spacing of the concave line is constant at 0.6  $\mu\text{m}$ . The streaks that extend in the *x*-direction are the pct//*x* seen in Fig. 4(d). These observed results are consistent with the results for the coconut crab's claw, CL [9]. Figs. 5 and 6 show SEM micrographs in the rear cephalothorax (RC) and the thinnest abdomen (AM). SEM micrographs in the front cephalothorax (FC) are shown in Fig. S2. As shown in Figs. 4–6 and Fig. S2, the tissue structure of the FC, RC, and AM observed from the fracture surface is almost the same as that of the 1WL and CL [9]. However, the *Sh* in the exocuticle and the microstructure observed from the polishing surface in the endocuticle are sufficiently different from those of the 1WL and CL [9]. The *Sh* in the cephalothorax and abdomen is greater than that in the 1WL, and it appears to decrease as it approaches the surface (Figs. 5(e) and 6(e) and Fig. S2(e)). The results indicate that the microstructures of the FC, RC, and AM, are characterized by a much coarser structure than that of the 1WL, shown in Fig. 4(e). In the endocuticle (Figs. 5(f) and 6(f))

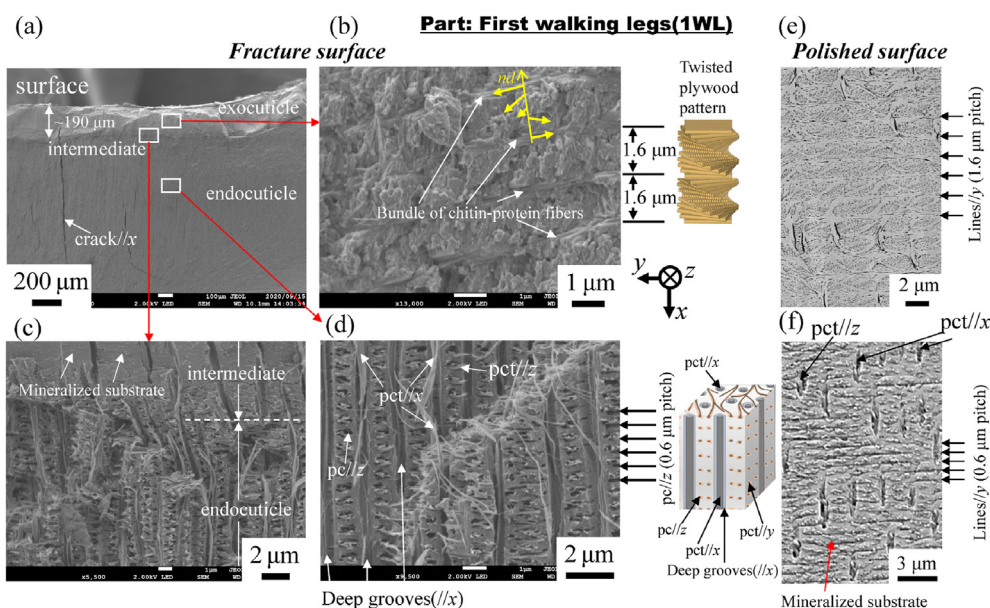


**Fig. 4.** SEM micrograph of the (a) fracture surface of the first walking leg. Enlarged SEM micrographs of the area enclosed by the rectangles in (a); (b) exocuticle layer, (c) intermediate layer, and (d) endocuticle layer. In (b), superimposed planes rotate around the normal axis (*nd*) of the exocuticle. SEM micrographs of the (e) exocuticle layer and (f) endocuticle layer on a polished surface. Here, pct denotes pore canal tubules, and pc denotes pore canals.

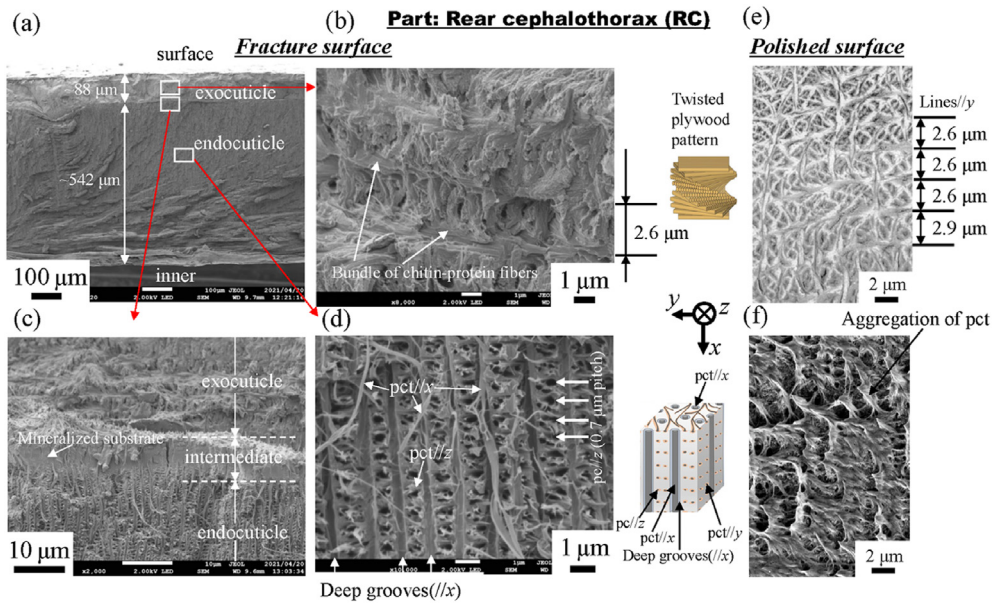


Fig. 5. SEM micrograph of (a) a fracture surface of the abdomen. Enlarged SEM micrographs of the area enclosed by the rectangles in (a); (b) exocuticle layer, (c) intermediate layer, and (d) endocuticle layer. SEM micrographs of (e) the exocuticle layer and (f) endocuticle layer on a polished surface.

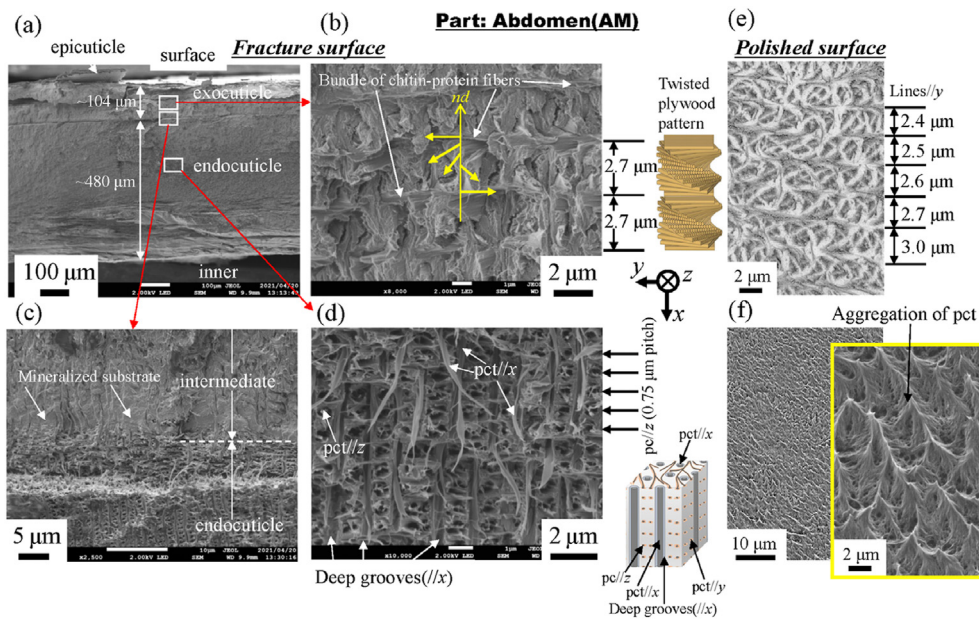


Fig. 6. SEM micrograph of the (a) fracture surface of the abdomen. Enlarged SEM micrographs of the area enclosed by the rectangles in (a); (b) exocuticle layer, (c) intermediate layer, and (d) endocuticle layer. SEM micrographs of the (e) exocuticle layer and (f) endocuticle layer on a polished surface.

and Fig. S2(f), almost no inorganic layer was observed, and the surface was covered by pct.

### 3.3. Hardness and stiffness

Table 2 shows the nanoindentation test results. The load  $P$ -displacement  $u$  curves of each area on all parts are shown in Fig. S3 in the supplementary material. Under  $P_{max} = 5$  mN, the  $u$  is small (i.e. hard) in the exocuticle and large (i.e. soft) in the intermediate or the endocuticle. In all parts, the  $H$  is hardest (1.40~4.01 GPa) in the exocuticle and harder at near the surface than at the mid-thickness. The  $H$  of the exocuticle in the CL was 4~6 times that of the endocuticle, which is consistent with the results of the hardness obtained via Vickers hardness testing [9]. In the CL and the 1WL, the  $H$  was the lowest (0.41 GPa in the CL and

0.47 GPa in the 1WL) in the intermediate, but the softest layer in the FC, RC, and AD was in the endocuticle. In particular, the  $H$  of these layers showed very small values between 0.15 and 0.25 GPa. These differences in  $H$  are related to mineralization. Fig. 7 shows variations of  $H$  with Ca concentrations. Here, Ca concentrations in an area close to the surface (distance from the surface,  $x \approx 20$  μm) in the exocuticle were added as EDS results, and those in the CL, 1WL, FC, RC, and AM were 30.9, 31.0, 28.2, 27.2, and 26.5 (wt%), respectively.

### 4. Discussion

The results indicate that the exoskeleton of the coconut crab is mainly composed of a hard exocuticle and a soft endocuticle, and each part was essentially the same tissue structure. The exocuticle has a very dense

**Table 2**

Nanoindentation results of three layers for all samples. Here, the properties are the average values, including their standard deviation.

Sample	Layer	Distance from surface, $x$ ( $\mu\text{m}$ )	Hardness, $H$ (GPa)	Stiffness, $E_r$ (GPa)
Claw (CL)	Exocuticle (near the surface)	20	$3.87 \pm 0.14$	$56.0 \pm 1.06$
	Exocuticle(1/2t)	125	$2.4 \pm 0.13$	$47.3 \pm 2.11$
	Intermediate	280	$0.41 \pm 0.06$	$13.6 \pm 1.05$
	Endocuticle(1/2t)	1500	$0.61 \pm 0.04$	$18.1 \pm 0.88$
First walking leg (1WL)	Exocuticle (near the surface)	20	$3.60 \pm 0.15$	$61.3 \pm 0.44$
	Exocuticle(1/2t)	110	$2.91 \pm 0.21$	$61.6 \pm 1.62$
	Intermediate	255	$0.47 \pm 0.03$	$16.5 \pm 0.74$
	Endocuticle(1/2t)	600	$0.70 \pm 0.09$	$22.9 \pm 1.57$
Front cephalothorax (FC)	Exocuticle (near the surface)	18	$4.01 \pm 0.24$	$68.1 \pm 3.21$
	Exocuticle(1/2t)	50	$2.60 \pm 0.26$	$46.1 \pm 2.20$
	Intermediate	125	$0.47 \pm 0.09$	$15.3 \pm 1.34$
	Endocuticle(1/2t)	350	$0.25 \pm 0.04$	$9.19 \pm 0.86$
Rear cephalothorax (RC)	Exocuticle (near the surface)	18	$2.86 \pm 0.33$	$56.3 \pm 3.72$
	Exocuticle(1/2t)	50	$1.40 \pm 0.07$	$33.3 \pm 1.38$
	Intermediate	80	$0.25 \pm 0.04$	$12.4 \pm 1.25$
	Endocuticle(1/2t)	350	$0.19 \pm 0.02$	$8.81 \pm 0.70$
Abdomen (AM)	Exocuticle (near surface)	18	$3.50 \pm 0.19$	$65.0 \pm 2.73$
	Exocuticle(1/2t)	50	$1.61 \pm 0.31$	$33.1 \pm 3.80$
	Intermediate	100	$0.40 \pm 0.04$	$14.16 \pm 1.08$
	Endocuticle(1/2t)	250	$0.15 \pm 0.03$	$9.42 \pm 1.16$

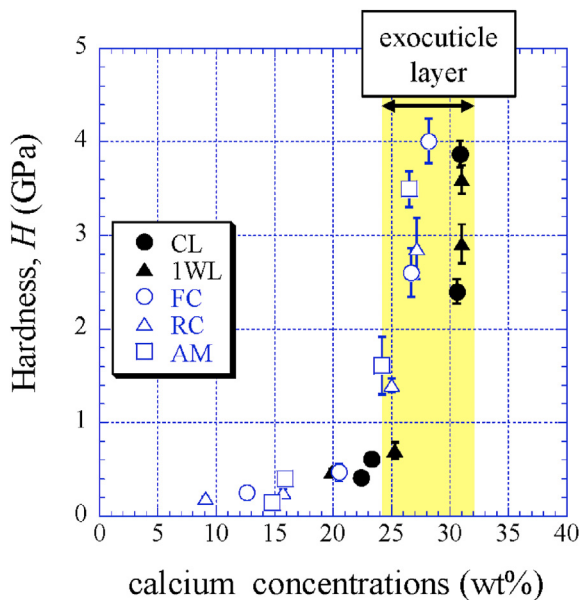


Fig. 7. Variations of hardness,  $H$ , with calcium concentrations.

twisted plywood structure with high Ca concentrations and high stiffness in the range of 33.1–68.1 GPa. The endocuticle showed a coarser structure without a twisted plywood pattern and a small stiffness of 8.81–22.9 GPa. The high  $H$  of the exocuticle is the result of stronger calcification as compared to that of the two layers, and the Ca concentrations ranging from 24.2 to 31.0 (wt%) in the exocuticle are consistent with those in the exocuticle of the other crabs [15]. The  $Sh$  of the twisted plywood structure, the exoskeleton thickness, and the thickness at each layer are significantly different by body part.

#### 4.1. Effect of the stacking height of the twisted plywood pattern structure

As shown in Figs. 4–6 and Fig. S2, the  $Sh = 1.6 \mu\text{m}$  in the 1WL was smaller than the  $Sh = 1.9 \mu\text{m}$  in the FC, the  $Sh = 2.6 \mu\text{m}$  in the RC, the  $Sh = 2.7 \mu\text{m}$  in the AM, and the  $Sh = 2.3 \mu\text{m}$  at mid-thickness of the exocuticle in the CL [9]. In Table 2, the  $H$  in the exocuticle was different near the surface and mid-thickness, although there was no significant difference in Ca concentrations, as shown in Fig. 7. If the stacking height of the twisted plywood structure is related to the hardness or stiffness, the

$Sh$ ,  $H$ , and  $E_r$  may have some correlation. Fig. 8 shows relationships between  $H$ ,  $E_r$ , and  $Sh$  in the exocuticle for all parts. The  $Sh$  near the surface and at mid-thickness in the exocuticle was analyzed via SEM micrographs on the polished surface. The analytical results in the CL and 1WL are shown in Fig. S4 and these in the FC, RC, and AM are shown in Fig. S5. From Fig. 8, we find that  $H$  increases with decreasing  $Sh$ , and the  $H$ – $Sh$  has a clear correlation as compared to  $E_r$ – $Sh$ . This result suggests that the  $Sh$  observed via an SEM from a fractured surface or a polished surface is one index for estimating hardness under the same Ca concentrations. In the exoskeleton of the American lobster, *Homarus americanus* [12]; the edible crab, *Cancer pagurus* [6]; the sheep crab, *Loxorhynchium grandis*; and the Dungeness crab, *Cancer magister* [16]; a twisted plywood structure and a stacking height of its pattern were clearly observed on a fracture surface. This was the same for coconut crabs, as shown in the 1WL (Fig. 4(b)), the RC (Fig. 5(b)), the FC (Fig. S2(b)), and the AM (Fig. 6(b)), and the CL (Fig. 3(b) in Inoue et al. [9]). Curiously, a twisted plywood structure could not be observed in the coconut club's endocuticle. Furthermore, some fracture surfaces consisted of terrace// $z$  and step// $x$  in the exocuticle (Fig. S6). Such a fracture surface provides mechanical resistance to avoid catastrophic failure [17,18]. Surprisingly, these step sizes corresponded to the  $Sh$ . In the future, we plan to examine the relationship between fracture characteristics and  $Sh$  through fracture tests.

#### 4.2. Differences in endocuticle of body parts

In the endocuticle shown in Figs. 4(d,f), 5(d), 6(d) and Fig. S2(d), the spacing of the pore canal parallel to  $z$  ( $pc//z$ ) was  $0.75 \mu\text{m}$  for the CL [9],  $0.60 \mu\text{m}$  for the 1WL,  $0.80 \mu\text{m}$  for the FC,  $0.70 \mu\text{m}$  for the RC, and  $0.75 \mu\text{m}$  for the AM. As a result, this spacing was in the range of 0.6–0.8  $\mu\text{m}$ , and there was no significant difference between the parts. However, the inorganic layer (Fig. 4(f)), seen on the polished surface of the 1WL and the CL [9], was hardly observed in the FC, RC, and AM, and the surface was covered by chitin protein of pct (Figs. 5(f), 6(f) and 2(f)). In the exoskeleton of the FC, RC, and AM, shown in Table 1, the Ca concentrations were lower than those in the CL and the 1WL; furthermore, the Ca concentrations in the endocuticle were extremely low as compared with those in the exocuticle. That is, the endocuticle in the cephalothorax and the abdomen is not strongly mineralized as compared to that in the claw and the walking legs. Fig. 9 shows the differences in the density of each part. The density of the exoskeleton was smaller than that,  $2.71 \text{ g/cm}^3$  [19], of general calcium carbonate ( $\text{CaCO}_3$ ) because many pores existed, and chitin fibers in the protein matrix are included in the exoskeleton.

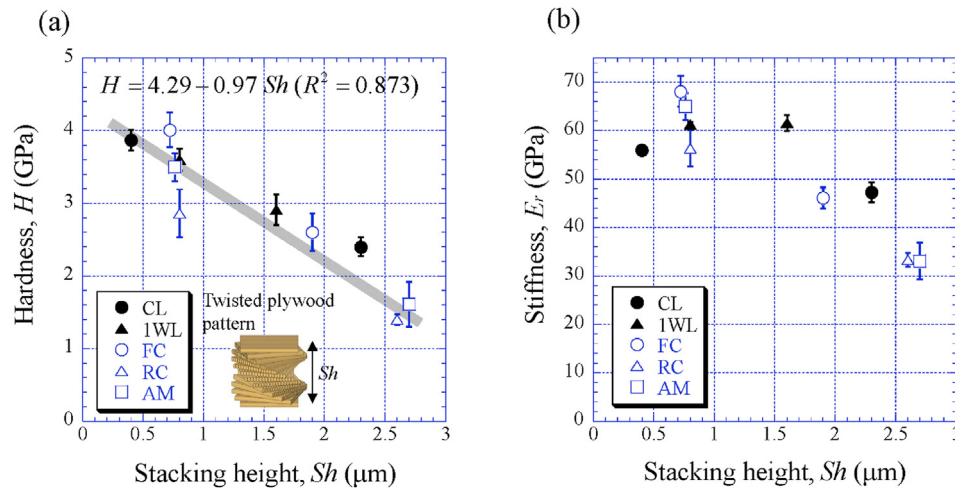


Fig. 8. Variations of (a) hardness,  $H$ , and (b) reduced stiffness,  $E_r$ , against the stacking height,  $Sh$ , of the twisted plywood pattern structure of the exocuticle layer.

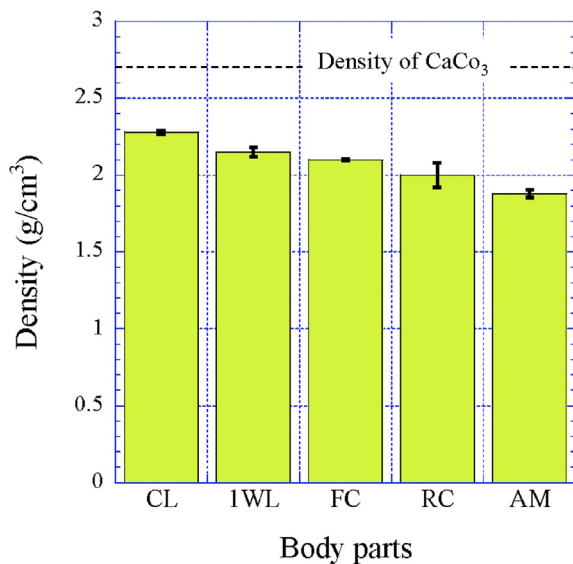


Fig. 9. True density of the exoskeleton of each part as measured by a pycnometer method.

The density of the CL was the highest, and that of the AM was the lowest. As shown in Figs. 5(f) and 6(f), due to a higher volume fraction of chitin protein, the inorganic layer was peeled off during polishing. Hence, the  $H$  and  $E_r$  at the endocuticle in the FC, RC, and AM showed very small values as compared with those in the CL and the 1WL. The  $E_r$  between 8.8 and 9.4 GPa shown in Table 2 is consistent with Young's modulus, 8.6–10 GPa, obtained from the tensile test of chitin fiber extracted from shrimp shells using ionic liquids [20].

#### 4.3. Hardness–stiffness balance

As shown in Table 2, for all parts, the hardness and stiffness of the exoskeleton of the coconut crab decreased steeply at the intermediate layer. In order to compare the coconut crab with other organisms in terms of mechanical properties, we attempted to plot the results obtained in the present study on a map of hardness and stiffness, which is one index of the abrasion resistance of materials. The results described in Table 2 are shown on the  $H$ – $E$  map in Fig. 10, including data for engineering materials families (metals, ceramics, and polymers) and other organisms

(the claw of the American lobster [12]; the carapace of the European edible crab [5]; the fang of the spider, *Cupiennius salei* [14]; the hammer of the stomatopod dactyl club of *Odontodactylus scyllarus* [13]; the scorpion's pincer [21]; and the jaw of the bloodworm, *Glycera dibranchiata* [11]). Based on Hertzian contact mechanics, the material property group that characterizes resistance to plastic deformation during contact with an abrasive can be ascertained. In the absence of a tangential load, the normal load,  $P_y^0$ , for yielding is given by

$$\frac{P_y^0}{R^2} = C_1 \left( \frac{H^3}{\bar{E}^2} \right) \left( 1 + \frac{\bar{E}'}{\bar{E}} \right)^2 \quad (1)$$

with  $C_1 = 0.8$ . Here,  $R$  and  $\bar{E}'$  is the mean curvature and the plane strain modulus of the abrasive, respectively, and  $\bar{E}$  is the plane strain modulus of the plate material. In many cases,  $\bar{E}' \gg \bar{E}$ , so that an elastic mismatch parameter,  $(1 + \bar{E}'/\bar{E})$ , is close to unity and thus Eq. (1) can be re-written in the simple form:

$$\frac{P_y^0}{R^2} \approx C_1 \left( \frac{H^3}{\bar{E}^2} \right) \quad (2)$$

Here, the failure load, characterized by  $P_y^0/R^2$ , is proportional to the material property group. Abrasion damage by localized plastic deformation corresponding to this guideline is illustrated in Fig. 10. As shown in Fig. S3, since nanoindentation load gradually increases with displacement in all layers, Eq. (2) is applicable. Data lying on a straight line of  $H^3/\bar{E}^2$  shown in Fig. 10 indicate materials with equivalent performances on the resistance of abrasion [22]. Interestingly, data of the endocuticle layer and the intermediate layer of the coconut crab are comparable to those of all polymers and some metals, and data of the exocuticle layer are higher than those of all polymers and are comparable to hard metallic alloys and soft ceramics. The map reveals that the values of  $H^3/\bar{E}^2$  in the exocuticle layer of the coconut crab are vastly superior and are similar to those of the stomatopod's hammer and the bloodworm's jaws positioned as top-class among organisms. Besides, the  $H$ – $E$  balance of the exocuticle layer of coconut crab is the best. In the stomatopod and the bloodworm, the superior properties have only very thin/very small areas near the surface of their important parts (hammers and jaws) for eating. The body of the coconut crab is larger, and the exocuticle layer is thicker as compared to the area of these organisms. In particular, the size of the claw was 79.2 mm (CL)  $\times$  39.8 mm (CH) [9] in the present crab, and the thickness of the exocuticle was 250  $\mu$ m. The exocuticle of the coconut crab is a very important layer for deterring predators and consuming a wide variety of relatively rigid food.

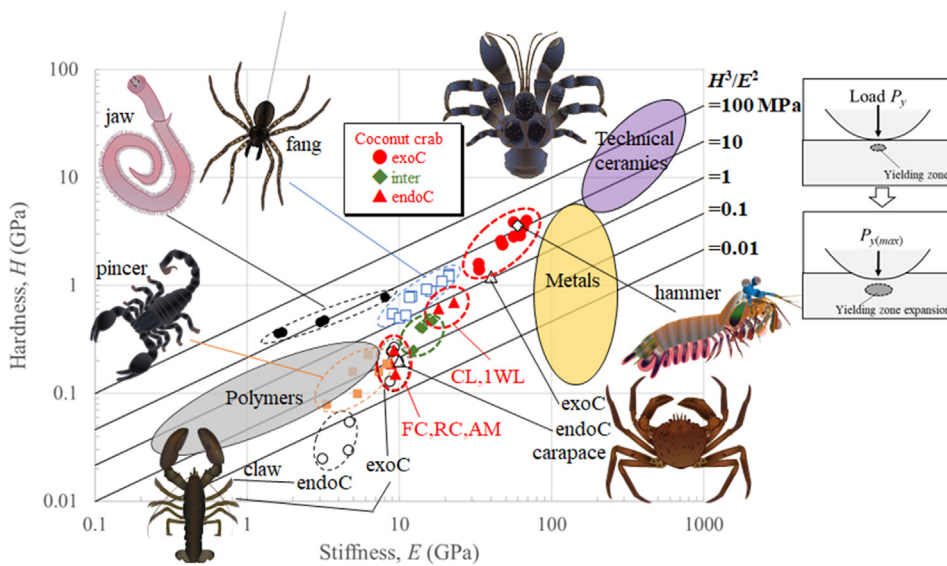


**Fig. 10.** Property maps for abrasion resistance, including data of various organisms and engineering materials. Body parts of the coconut crab (CL: claw; 1WL: first walking leg; FC: front cephalothorax; RC: rear cephalothorax; AM: abdomen). Exoskeleton (exoC: exocuticle layer; endoC: endocuticle layer; inter: intermediate layer). Compared arthropods (American lobster's claw [12]; European edible crab's carapace [5]; Spider's fang [14]; Stomatopod's hammer [13]; Scorpion's pincer [21]; Bloodworm's jaw [11]).

## 5. Conclusion

The tissue structures, chemical compositions, and mechanical properties of the exoskeleton of the claw, the first walking leg, the cephalothorax, and the abdomen of the coconut crab were compared. The main results are as follows:

- (1) The exoskeleton composed of a hard exocuticle and a soft endocuticle has essentially the same tissue structure regardless of the body part. The exocuticle has a very dense twisted plywood structure with a high Ca concentration and high stiffness. The endocuticle showed a coarser structure without a twisted plywood pattern and low stiffness.
- (2) The stacking height,  $Sh$ , of the twisted plywood structure in the exocuticle, the exoskeleton thickness, and the thickness of each layer were significantly different by body part. The claw and legs were thicker than the cephalothorax and abdomen.
- (3) The  $Sh$  decreases and the hardness ( $H$ ) increases as it approaches the surface. The hardness ( $H$ ) and  $Sh$  had a relation of  $H = 4.29 - 0.97 Sh$ . The  $Sh$  observed in the exocuticle of coconut crabs may be one index for estimating hardness.
- (4) The exocuticle is strongly mineralized regardless of body parts. The endocuticle in the cephalothorax and the abdomen was not strongly mineralized as compared to that in the claw and the walking legs.
- (5) The exocuticle layer of the coconut crab has an excellent hardness–stiffness balance and has the highest abrasion resistance in the phylum arthropod.

## Author contributions

**Tadanobu Inoue:** Conceptualization, Methodology, Investigation, Data Curation, Writing - Original Draft, Writing - Review & Editing, Visualization, Project administration, Funding acquisition. **Toru Hara:** Writing - Review & Editing, Visualization. **Koji Nakazato:** Data Curation, Resources. **Shin-ichiro Oka:** Resources, Writing - Review & Editing, Visualization.

## Declaration of competing interest

The authors declare that they have no known competing financial interests or personal relationships that could have appeared to influence the work reported in this paper.

## Acknowledgments

We thank Ms. Y. Hara and Ms. Y. Kashiwara for their experimental assistance with the microstructural observations and illustrations. This study was supported by JSPS KAKENHI Grant Number JP21H04537, Japan; The Uehara Memorial Foundation, Japan; Iketani Science and Technology Foundation (Grant No.0331136-A), Japan. The grants are greatly appreciated.

## Appendix A. Supplementary data

Supplementary data to this article can be found online at <https://doi.org/10.1016/j.mtbio.2021.100132>.

## References

- [1] B. Zhang, Q. Han, J. Zhang, Z. Han, S. Niu, L. Ren, Advanced bio-inspired structural materials: local properties determine overall performance, *Mater. Today* 41 (2020) 177–199, <https://doi.org/10.1016/j.mattod.2020.04.009>.
- [2] J.F. Vincent, Survival of the cheapest, *Mater. Today* 5 (12) (2002) 28–41, [https://doi.org/10.1016/S1369-7021\(02\)01237-3](https://doi.org/10.1016/S1369-7021(02)01237-3).
- [3] S. Nikolov, M. Petrov, L. Lympirakis, M. Friák, C. Sachs, H.-O. Fabritius, D. Raabe, J. Neugebauer, Revealing the design principles of high-performance biological composites using Ab initio and multiscale simulations: the example of lobster cuticle, *Adv. Mater.* 22 (2010) 519–526, <https://doi.org/10.1002/adma.200902019>.
- [4] S. Pradhan, A.K. Brooks, V.K. Yadavalli, Nature-derived materials for the fabrication of functional biodevices, *Mater Today Bio.* 7 (2020) 100065, <https://doi.org/10.1016/j.mtbio.2020.100065>.
- [5] H.-O. Fabritius, E.S. Karsten, K. Balasundaram, S. Hild, K. Huemer, D. Raabe, Correlation of structure, composition and local mechanical properties in the dorsal carapace of the edible crab *Cancer pagurus*, *Z. Kristallogr.* 227 (2012) 766–776, <https://doi.org/10.1524/zkri.2012.1532>.
- [6] F. Boßelmann, P. Romano, H. Fabritius, D. Raabe, M. Epple, The composition of the exoskeleton of two crustacea: the American lobster *Homarus americanus* and the edible crab *Cancer pagurus*, *Thermochim. Acta* 463 (2007) 65–68, <https://doi.org/10.1016/j.tca.2007.07.018>.
- [7] W.D. Coffey, J.A. Nardone, A. Yarram, W.C. Long, K.M. Swiney, R.J. Foy, G.H. Dickinson, Ocean acidification leads to altered micromechanical properties of the mineralized cuticle in juvenile red and blue king crabs, *J. Exp. Mar. Biol. Ecol.* 495 (2017) 1–12, <https://doi.org/10.1016/j.jembe.2017.05.011>.
- [8] C. Sachs, H. Fabritius, D. Raabe, Experimental investigation of the elastic–plastic deformation of mineralized lobster cuticle by digital image correlation, *J. Struct. Biol.* 155 (2006) 409–425, <https://doi.org/10.1016/j.jsb.2006.06.004>.
- [9] T. Inoue, S. Oka, T. Hara, Three-dimensional microstructure of robust claw of coconut crab, one of the largest terrestrial crustaceans, *Mater. Des.* 206 (2021) 109765, <https://doi.org/10.1016/j.matdes.2021.109765>.
- [10] S. Oka, K. Miyamoto, S. Matsuzaki, T. Sato, Growth of the coconut crab, *Birgus latro*, at its northernmost range estimated from Mark–Recapture using individual identification based on carapace grooving patterns, *Zool. Sci.* 32 (2015) 260–265, <https://doi.org/10.2108/zs150008>.

- [11] D.N. Moses, M.A. Mattoni, N.L. Slack, J.H. Waite, F.W. Zok, Role of melanin in mechanical properties of *Glycera* jaws, *Acta Biomater.* 2 (2006) 521–530, <https://doi.org/10.1016/j.actbio.2006.05.002>.
- [12] D. Raabe, C. Sachs, P. Romano, The crustacean exoskeleton as an example of a structurally and mechanically graded biological nanocomposite material, *Acta Mater.* 53 (2005) 4281–4292, <https://doi.org/10.1016/j.actamat.2005.05.027>.
- [13] J.C. Weaver, G.W. Milliron, A. Miserez, K.E. Lutterodt, S. Herrera, I. Gallana, W.J. Mershon, B. Swanson, P. Zavattieri, E. DiMasi, D. Kisailus, The stomatopod dactyl club: a formidable damage-tolerant biological hammer, *Science* 336 (2012) 1275–1280, <https://doi.org/10.1126/science.1218764>.
- [14] Y. Politi, M. Prieuwater, E. Pippel, P. Zaslansky, J. Hartmann, S. Siegel, C. Li, F.G. Barth, P. Fratzl, A Spider's Fang: how to design an injection needle using chitin-based composite material, *Adv. Funct. Mater.* 22 (2012) 2519–2528, <https://doi.org/10.1002/adfm.201200063>.
- [15] F. Nekvapil, S.C. Pinzaru, L.B. Tudoran, M. Suci, B. Glamuzina, T. Tamaş, V. Chiş, Color-specific porosity in double pigmented natural 3d-nanoarchitectures of blue crab shell, *Sci. Rep.* 10 (2020) 3019, <https://doi.org/10.1038/s41598-020-60031-4>.
- [16] P.-Y. Chen, A.Y. Lin, J. McKittrick, M.A. Meyers, Structure and mechanical properties of crab exoskeletons, *Acta Biomater.* 4 (2008) 587–596, <https://doi.org/10.1016/j.actbio.2007.12.010>.
- [17] S. Deville, E. Saiz, R.K. Nalla, A.P. Tomsia, Freezing as a path to build complex composites, *Science* 311 (2006) 515–518, <https://doi.org/10.1126/science.1120937>.
- [18] T. Inoue, Y. Kimura, S. Ochiai, Shape effect of ultrafine-grained structure on static fracture toughness in low-alloy steel, *Sci. Technol. Adv. Mater.* 13 (2012), 035005, <https://doi.org/10.1088/1468-6996/13/3/035005>.
- [19] T. Matschei, B. Lothenbach, F.P. Glasser, The role of calcium carbonate in cement hydration, *Cement Concr. Res.* 37 (2007) 551–558, <https://doi.org/10.1016/j.cemconres.2006.10.013>.
- [20] Y. Qin, X. Lu, N. Sun, R.D. Rogers, Dissolution or extraction of crustacean shells using ionic liquids to obtain high molecular weight purified chitin and direct production of chitin films and fibers, *Green Chem.* 12 (2010) 968–971, <https://doi.org/10.1039/C003583A>.
- [21] I. Kellersztein, S.R. Cohen, B. Bar-On, H.D. Wagner, The exoskeleton of scorpions' pincers: structure and micro-mechanical properties, *Acta Biomater.* 94 (2019) 565–573, <https://doi.org/10.1016/j.actbio.2019.06.036>.
- [22] F.W. Zok, A. Miserez, Property maps for abrasion resistance of materials, *Acta Mater.* 55 (2007) 6365–6371, <https://doi.org/10.1016/j.actamat.2007.07.042>.